Soft Matter

Cite this: *Soft Matter*, 2012, **8**, 10732

www.rsc.org/softmatter

PAPER

Microdroplet impact at very high velocity

Claas Willem Visser,* Yoshiyuki Tagawa, Chao Sun* and Detlef Lohse*

Received 7th June 2012, Accepted 13th July 2012
DOI: 10.1039/c2sm26323h

Water microdroplet impact at velocities up to 100 m s^{-1} for droplet diameters ranging from 12 to 100 μm is studied. This parameter range covers the transition from capillary-limited to viscosity-limited spreading of the impacting droplet. Splashing is absent for all measurements; the droplets always gently spread over the surface. The maximum spreading radius is compared to several existing models. The model by Pasandideh-Fard *et al.* agrees well with the measured data, indicating the importance of a thin boundary layer just above the surface, in which most of the viscous dissipation in the spreading droplet takes place. As explained by the initial air layer under the impacting droplet, a contact angle of 180 degrees is used as the model input.

I. Introduction

High-pressure spray cleaning, droplet–wall interactions in diesel engines, and plasma spraying are notable examples of processes in which high-speed impact of small droplets on a solid surface is a key phenomenon. In these applications, droplets with a characteristic size of 1 to 100 μm and a velocity of the order 100 m s^{-1} impact on a solid surface.[2–4] Despite this industrial interest, microscale droplet impact at very high velocities (U_0 > 50 m s^{-1}) has only been studied for solidifying metal droplets.[5] This is mainly due to the challenging parameter regime: very high spatial and temporal resolutions are required to study the relevant phenomena. In addition, it is difficult to create impact events at these velocities. An understanding of the phenomenon of high-speed micro-sized droplet impact is thus lacking.[6,7]

In this work, we aim to extend current results in three ways. First, we present a novel method for high-velocity droplet generation, by using a system to create ultrafast liquid jets. Second, using high-speed imaging, the impact dynamics are studied. Third, a quantitative investigation of the maximum spreading radius will be presented and compared to existing models, to improve our understanding of droplet spreading.

II. Parameter space

To compare our results with previous work, a phase diagram of the droplet size (D_0) and impact speed (U_0) is plotted in Fig. 1(a). Most work up to now has focused on impact dynamics of droplets with a size of ~1 mm diameter. The studies on micro-droplet impact were mainly at relatively low speeds (up to 10 m s^{-1}).[5,8,9] Our study connects these previous investigations, in particular those on water microdroplets at lower velocities[8] and metal microdroplet impact at very high velocities.[5]

Fig. 1(b) shows a phase diagram of the achieved Reynolds and Weber numbers in experimental droplet studies. The Weber number is defined as $We = \rho D_0 U_0^2/\sigma$, where σ is the surface tension and ρ is the density. The Reynolds number is given by $Re = \rho D_0 U_0/\mu$ where μ represents the dynamic viscosity. As shown in

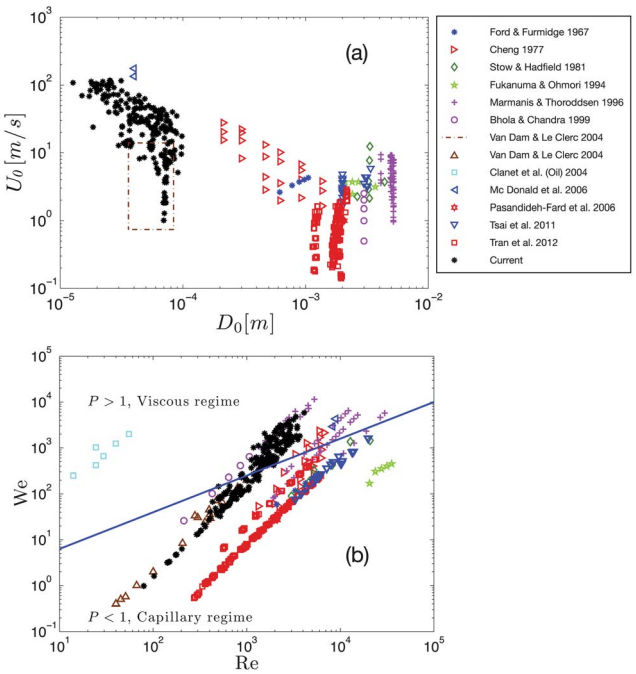

Fig. 1 Parameter space of (a) droplet velocities and radii and (b) Weber and Reynolds numbers for various droplet impact experiments.[1,5,8–17] The solid blue line signals $P = 1$ (P is defined as $P = We/Re^{4/5}$ by Clanet *et al.*[10]) and separates the capillary regime with $P < 1$ from the viscous regime with $P > 1$.

Physics of Fluids Group, Faculty of Science and Technology, J. M. Burgers Centre for Fluid Dynamics, University of Twente, The Netherlands. E-mail: c.visser@utwente.nl; c.sun@utwente.nl; d.lohse@utwente.nl

Fig. 1(b), the Re–We values of our measurements largely overlap with previous data. However, our data have been taken for microdroplets instead of mm sized droplets as indicated in Fig. 1(a). As the droplet size is a key control parameter for impact dynamics, various models developed to describe the mm sized droplet impact may not hold for microdroplet impact dynamics. The large impact velocity also explains why our data have relatively high Weber numbers for the given Reynolds numbers.

Our data cover the transition from the capillary- to the viscosity-dominated limits of droplet spreading,[10] as shown by the solid line in Fig. 1(b) (an explanation of this transition is provided below). So far, to investigate this transition, liquids of different viscosities and surface tensions were required in order to achieve a sufficient coverage of the Re–We parameter space. Using droplets of microscopic scales lowers the Weber number for which this transition takes place, allowing us to study the transition region with a single liquid.

III. Experimental setup

To create high-velocity microdroplets ($U_0 \geq 10$ m s^{-1}), we make use of a new method to create ultrafast liquid jets,[18] as sketched in Fig. 2(a). In a nutshell, the method works as follows. By focusing a laser pulse with a microscope objective, a vapor bubble is created in a capillary tube, by laser-induced cavitation. From this bubble, a shock wave travels to the meniscus, which in turn forms a liquid jet, thanks to flow focusing. Subsequently, this jet breaks up into tiny droplets with a velocity similar to the jet velocity (Fig. 2(b)).

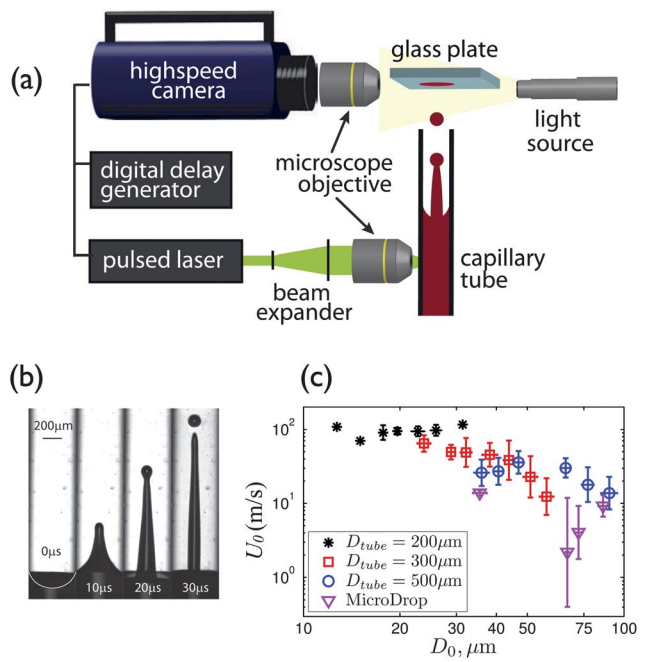

Fig. 2 (a) Setup used for the generation of fast droplets. (b) Jet generation and breakup at different instants. (c) Ranges of the achieved droplet velocities and radii for different droplet generator settings. Capillary tube diameters are decreased from 500 μm to 200 μm to generate smaller and faster droplets. In addition, to create slow droplets, a MicroDrop apparatus is used. As approximately 230 measurements were performed, the data are binned. The bars represent one standard deviation.

It is found that the tube diameter is a key control parameter for both the jet diameter and the jet tip velocity.[18] Therefore, capillaries with different diameters are used to create a range of droplet sizes and velocities. In addition, the laser energy and the distance between the laser focus and the meniscus are varied to generate droplets at different velocities for a given tube diameter,[18] resulting in the diameter and velocity ranges, as shown in Fig. 2(c). With this method, approximately 170 droplet impacts on a dry surface were examined. For the sake of clarity, the data are binned in the figure.

To create droplets at velocities between 1 and 10 m s^{-1}, a commercially available Microdrop dispenser (MD-140-752, Microdrop technologies, Germany) is used. By varying the input voltage between 60 V and 160 V per pulse, a range of velocities is covered. The droplet diameter ranges from 40 μm to 80 μm, as shown in Fig. 2(c).

A standard microscope slide was used as an impact plate, which is placed above the tip of the capillary tube. Atomic force microscope measurements indicated a roughness R_a below 10 nm. The droplet impact is visualized from the side. After each impact measurement, the glass plate was cleaned with ethanol and dried with paper tissue. Frequent checks with a 10× optical microscope (after the cleaning procedure) indicated that this method usually resulted in an optically clean surface, *i.e.*, hardly any paper fibers or dirt were sticking to the surface. To increase the absorption rate of the green laser, the liquid used in the present work was a standard water-based blue inkjet printer ink, with density $\rho = 998$ kg m^{-3}, surface tension $\sigma = 72$ mN m^{-2}, and viscosity $\mu = 10^{-3}$ Pa s.

Magnifications of 10× to 40× are obtained by combining a standard Olympus 10× objective with an adjustable 12× zoom lens (Navitar 1-50015). An Olympus ILP-1 light source is used for illumination. An ultra high-speed camera (Shimadzu HPV-1) is used to study the microdroplet impact dynamics, at recording rates of 1.25 × 10^5 to 10^6 frames per second. For the fastest droplets ($U_0 \approx 100$ m s^{-1}), the impact duration is approximately $\tau = D_0/U_0 \approx 0.2$ μs, which is below the temporal resolution of the camera. Thus, complete capturing of such events requires even higher frame rates[19] or pulsed illumination, *e.g.* as used in ref. 20. However, these techniques require a level of control of the moment of impact which is not achieved with the present setup. The high-speed camera has a minimum shutter time of 500 ns. Therefore, at high impact velocities, substantial motion blur is observed (*e.g.* Fig. 3(c)), as the shutter time approaches τ. Still, with the current setup, the presence of splashing could be assessed and the maximum spreading radius could be observed in an entirely new parameter regime.

Special care was taken to ensure that the data analysis was reliable and consistent. First, the raw Shimadzu movie files were read into Matlab. The relevant frames of each movie, as well as the area of interest, were selected manually resulting in image sequences as shown in Fig. 3. After contrast-enhancement, the experiments were inspected manually and removed if the images were unclear. Then, in the first two frames of interest, the droplet was identified manually. Subsequently, a cross-correlation method between the sub-areas of the frames (these sub-areas, with a width of 3 times the droplet size and a height dependent on the velocity estimated, contain the droplet image) was used to determine the droplet position in each frame. From the

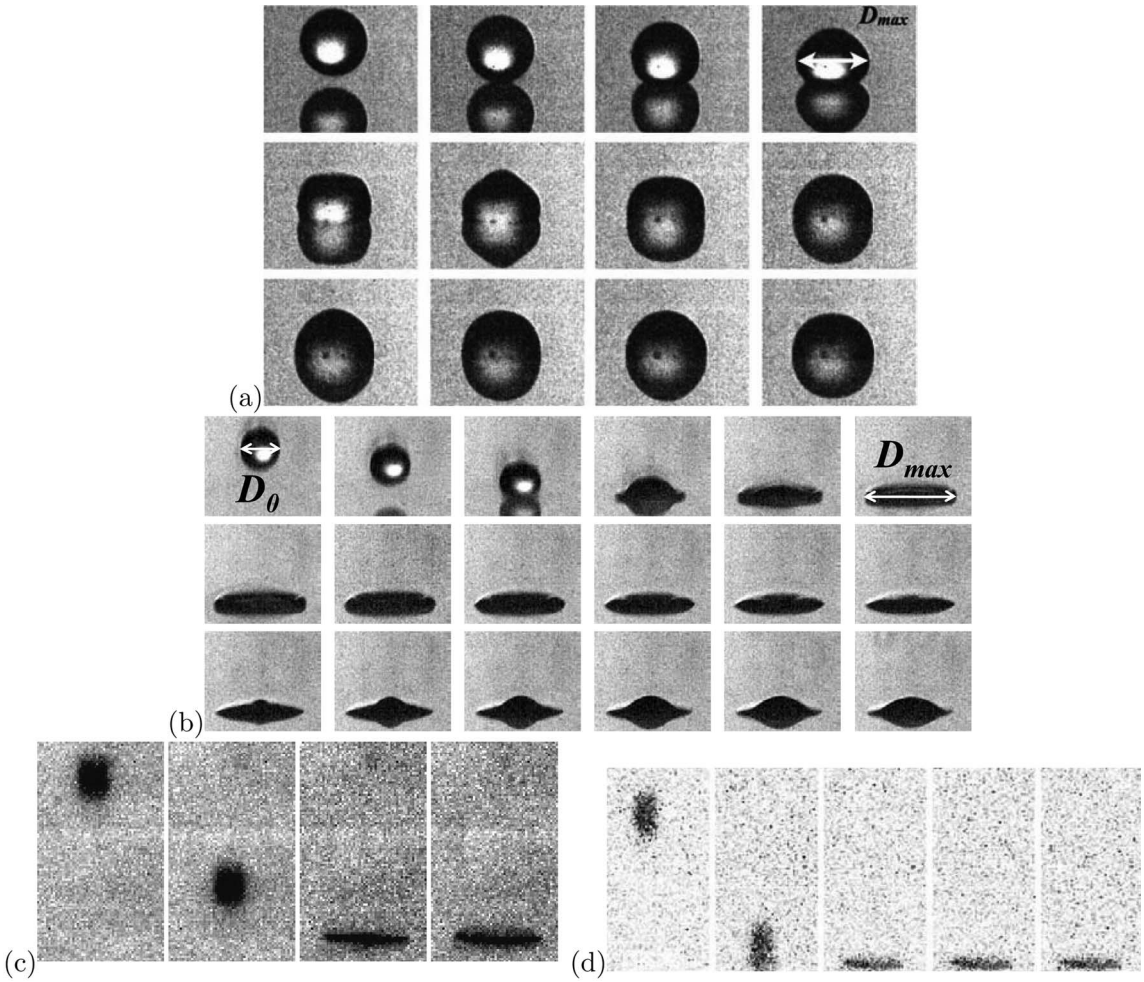

Fig. 3 Time series of droplet impacts at different impact velocities. (a) $U_0 = 0.7$ m s^{-1}, $D_0 = 70$ μm, We = 0.52, Re = 56, and the time lag δt between the frames is 8 μs. Droplet oscillations and air bubble entrapment can clearly be seen. (b) $U_0 = 7.7$ m s^{-1}, $D_0 = 71$ μm, We = 60, Re = 613, and $\delta t = 4$ μs. Spreading into a thin center sheet and a thicker rim are observed, followed by oscillations and partial withdrawal of fluid from the rim towards the droplet center. (c) $U_0 = 73$ m s^{-1}, $D_0 = 23$ μm, We $= 1.8 \times 10^3$, Re $= 1.9 \times 10^3$, and $\delta t = 1$ μs. The details of the spreading phase can no longer be resolved. (d) $U_0 = 100$ m s^{-1}, $D_0 = 20$ μm, We $= 3 \times 10^3$, Re $= 2.3 \times 10^3$, and $\delta t = 1$ μs.

correlation, the velocity was calculated. To determine the droplet size before and after spreading, the images were converted to black-and-white. Using standard Matlab methods, coherent structures were automatically labelled. Using thresholds for eccentricity and size, the droplet area was identified from the labeled areas. The width of the labeled area (a standard property in Matlab) then provided the droplet size. As a check, a diameter-sized bar was plotted over the centre of the droplet. The result was adjusted manually when necessary, to match the maximum droplet radius. In the graphs shown in Fig. 2c and 4, the data were binned. The error bars represent one standard deviation. Each data point in Fig. 4 (to be discussed below) contains at least 4 measurements.

IV. Results

A. Impact phenomenology

In general, the droplet impact process can be divided into the following phases. When the droplet approaches the solid surface, the air between the falling drop and the surface is strongly squeezed, leading to a pressure buildup in the air under the drop. The enhanced pressure results in a dimple formation in the droplet and an air layer development between the droplet and the target plate.[21–23] Before the droplet wets the surface, the liquid moves on top of this air cushion. The droplet extends in the radial direction until it reaches a maximum spreading radius. In this phase, splashing can occur.[7,16,21,24–26] Finally, the droplet completely wets the surface and an air bubble is entrapped.[23]

The first aim of this work is to assess the dynamics of micro-droplet impact, *i.e.* to find out whether the drop is in the splashing or gentle spreading regime. The latter one is defined by droplet deformation into a pancake shape, without satellite droplet formation. Time series of droplet impacts and the subsequent spreading phases are shown in Fig. 3. For these figures, the velocity ranges from 0.7 m s^{-1} to 100 m s^{-1}.

At low velocity ($U_0 = 0.7$ m s^{-1}), initial flattening of the droplet bottom is observed, as shown in Fig. 3(a). Subsequently, the droplet spreads over the substrate into a (virtually) half-dome

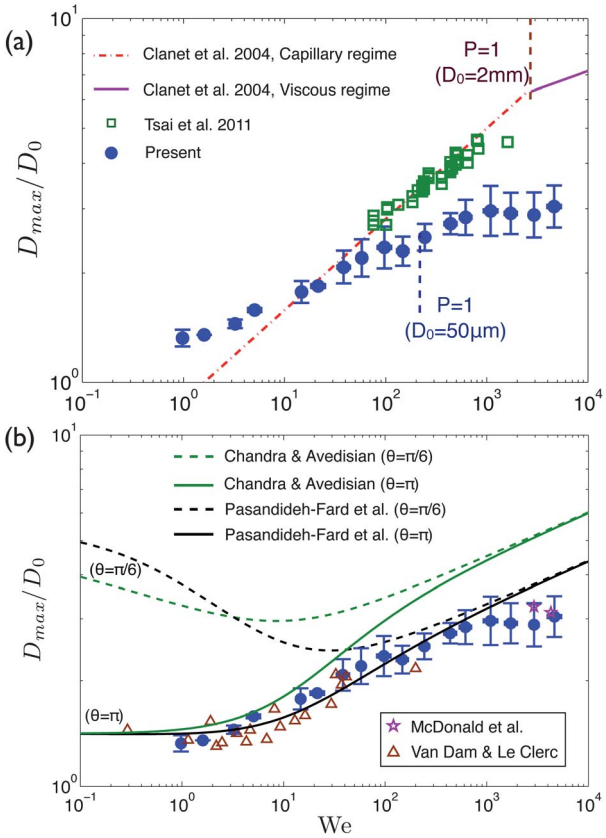

Fig. 4 The normalized maximum spreading D_{max}/D_0 *vs.* We. (a) Solid circles: the present microdroplet data. Open squares: mm sized droplet impact on superhydrophobic surfaces from Tsai *et al.*[16] Dashed-dotted line: the capillary model by Clanet *et al.*[10] Solid line: the viscous model by Clanet *et al.*[10] The short vertical dashed lines show the transitional Weber number We_t at $P = 1$ for a 2 mm sized droplet and for a 50 μm droplet. (b) Solid circles: the present microdroplet data. Stars: data from McDonald *et al.*[5] with impact of molten metal microdroplets. Open triangles: low-speed microdroplet impact experiments by Van Dam and Le Clerc.[8] Lines: model by Chandra and Avedisian[29] (dark-green lines) and the Pasandideh-Fard[1] model (black lines), evaluated for the initial diameter $D_0 = 50$ μm and contact angles π/6 (dashed lines) and π (solid lines).

shaped cap. During spreading, the droplet starts to oscillate and comes to rest only after the droplet has reached its maximum diameter. Additionally, air bubble entrainment is observed (the small black dot, just left of the droplet center). These phenomena are consistent with what had been reported in ref. 8, which includes a detailed discussion on the droplet oscillation frequency and the size and cause of the bubble/cushioning entrained.[16,22,23,27] At medium velocities (7.7 m s^{-1}, Fig. 3(b)), the droplet deforms into a disc-like structure. Here, the central impact area is a sheet-like structure surrounded by a thicker rim. Again, capillary oscillations were observed. Finally, even at very high velocities (Fig. 3(c) and (d)), no splashing is observed. Thus, we conclude that gentle impact occurs for all the velocities and droplet sizes investigated in the present work. Apart from the surrounding pressure and the surface roughness, the splashing dynamics of course also depends on the droplet size and for these small droplets the surface tension is strong enough to prevent splashing.

B. Maximum spreading

Now the maximum spreading radius will be determined and compared against various models. As knowledge of the maximum spreading diameter is of paramount importance for industrial applications, a plethora of models has been developed.[1,9,10,28–32] It is generally agreed that the spreading is limited by either viscosity or surface tension. Therefore, a key issue is to define which of these is dominant. To study this issue, we will first briefly summarize several models.

Assuming an inviscid liquid, the maximum spreading is limited by the surface tension. Balancing the Laplace pressure force with the inertial deceleration of the drop, a scaling of $D_{max}/D_0 \sim We^{1/4}$ is obtained.[9,10] This scaling is remarkably robust[10,14,16] in the capillary regime. As shown in Fig. 4(a), the data of mm sized droplet impact on superhydrophobic surfaces obtained by Tsai *et al.*[16] agree well with this 1/4 scaling law.

Another limiting case is to completely ignore surface tension and assume that the maximum spreading radius is limited by the viscous dissipation during droplet spreading.[10] This yields $D_{max}/D_0 \sim Re^{1/5}$ as scaling law, which holds well for mm sized droplets in the viscous regime as shown in ref. 10.

To quantify the transition between the viscous and the capillary regimes, Clanet *et al.*[10] defined the parameter $P = We/Re^{4/5}$. For $P < 1$, a surface-tension dominated regime is expected (*i.e.* $D_{max}/D_0 \sim We^{1/4}$), whereas a viscous scaling is predicted for $P > 1$, yielding the previously mentioned $D_{max}/D_0 \sim Re^{1/5}$. In Fig. 4(a), the transitional Weber number We_t, defined by $P = 1$, for droplets of $D_0 =$ 2 mm and 50 μm is plotted. For 2 mm sized droplets, $We_t \simeq 3 \times 10^3$, whereas it decreases to $We_t \simeq 2 \times 10^2$ for 50 μm sized ones. As shown in Fig. 4(a), the present microdroplet data are in between the transition regime from the capillary regime to the viscous regime. For a given We, the microdroplet spreading is lower than that for the mm sized droplets due to the viscous effects. This combination of two simple models provides a decent first description of the impact dynamics. However, more detailed models are possible and have been developed. As described by Chandra and Avedisian,[29] the dissipated energy equals the work done, and can thus be estimated by

$$W = \int_0^\tau \int_{V_\nu} \phi \approx V_\nu \tau \phi \approx V_\nu \tau \mu \left(\frac{U_0}{L}\right)^2 \quad (1)$$

where ϕ is the dissipation function, estimated as $\mu(U_0/L)^2$,[10,29] with τ being the typical impact timescale, $V_\nu = \pi L D_{max}^2$ the total droplet volume, and L the characteristic dissipation length scale, which in this model is selected as the height of the droplet splat h. In the model by Chandra and Avedisian,[29] W is used in an energy balance $E_k + E_s = W + E_s'$, where E_k is the kinetic energy, and E_s and E_s' are surface energies before and after impact, respectively. However, as shown by Pasandideh-Fard *et al.*[1] and our results, this model strongly overpredicts the maximum spreading radius.

The model was revisited by Pasandideh-Fard *et al.*[1] Their numerical simulations suggested that the dissipation takes place in a thin boundary layer within the expanding droplet, implying that the characteristic length scale L in the above eqn (1) is not the pancake thickness h but has to be replaced by the Prandtl–Blasius boundary layer thickness δ (ref. 1):

$$\delta = 2\,\frac{D_0}{\sqrt{\mathrm{Re}}}, \tag{2}$$

finally resulting in the following equation for D_{max}/D_0:

$$D_{max}/D_0 = \sqrt{\frac{\mathrm{We}+12}{3(1-\cos\theta)+4\left(\mathrm{We}/\sqrt{\mathrm{Re}}\right)}}. \tag{3}$$

Here, θ is the contact angle. At low impact velocities ($We \lesssim 10$) this model saturates, as the droplet impact can be considered to be effectively static and E_k and W vanish.

In Fig. 4(b), the measured maximum spreading of microdroplet impacts is plotted *versus* the Weber number. The maximum spreading is measured at the moment when the deformation of the droplet is maximum before it wets the surfaces, as shown in Fig. 3(a) and (b). At low velocities, the present data saturate around a spreading of ~1.3 times the initial diameter, which has a good overlap with previous low-speed microdroplet impact experiments.[8] At high velocities, spreading of only ~3 times the initial diameter is found for even the fastest droplets. This is consistent with (even faster) impact of molten metal microdroplets,[5] even though the liquid properties were very different from our experiments.

Fig. 4(b) is complemented with the models of Chandra and Avedisian[29] and Pasandideh-Fard *et al.*,[1] evaluated for an initial diameter of $D_0 = 50$ μm. We first examine the maximum spreading calculated from these models for two different contact angles, *i.e.* $\theta = \pi/6$ and π. The dashed lines in Fig. 4(b) clearly show that the contact angle of $\pi/6$ results in a much larger spreading factor for both the models as compared to the experimental data. As discussed above, an air layer is present between the spreading drop and the solid surface before the droplet wets the surface. First, it was shown that decreasing the air pressure can prevent splashing.[24] Later, the temporal evolution of the air layer has been experimentally measured[22] and investigated numerically.[21] The existence of the air layer implies a "contact angle" which would be best described by $\theta = \pi$. As shown by the solid lines in Fig. 4(b), this approach remarkably decreases the deviations between the experiments and the results of both models. A good agreement is found between the microdroplet data and the Pasandideh-Fard model[1] up to $We \approx 10^3$. This indicates the importance of a finite boundary layer thickness in the dissipation of spreading droplets in the present parameter regime. For $We > 10^3$, the increasing trend of D_{max}/D_0 *versus* We seems to saturate. This finding is consistent with ref. 9, and will be studied in future work.

V. Conclusions

The impact of water microdroplets on smooth solid surfaces is investigated experimentally. By using a new droplet-generating device, impact events were created at velocities ranging from 1 to 100 m s^{-1} with droplet diameters between 12 and 100 μm. This parameter regime covers the transition between surface tension- and viscosity-dominated spreading of the droplet. For all impact events, no splashing is observed. The maximum spreading radius was compared to several models. The model by Pasandideh-Fard *et al.*[1] performs best, indicating that boundary layer dynamics play a key role in droplet spreading. In addition, we find that an initial contact angle of 180 degrees should be used as the input value. This confirms the presence of an air layer under the impacting droplet.

Acknowledgements

We would like to acknowledge the support from the foundation for Fundamental Research of Matter (FOM). We thank Mark-Jan van der Meulen for help with the MicroDrop dispenser. James Seddon is thanked for AFM measurements of the glass impact plate. We thank C. Clanet, H. Lhuissier, D. van der Meer, A. Prosperetti, J. H. Snoeijer, and P. Tsai for stimulating discussions.

References

1 M. Pasandideh-Fard, Y. M. Qiao, S. Chandra and J. Mostaghimi, Capillary effects during droplet impact on a solid surface, *Phys. Fluids*, 1996, **8**, 650.
2 S. Mitra, Breakup Process of Plane Liquid Sheets and Prediction of Initial Droplet Size and Velocity Distributions in Sprays, PhD thesis, University of Waterloo, 2001.
3 J. Blaisot and J. Yon, Droplet size and morphology characterization for dense sprays by image processing: application to the Diesel spray, *Exp. Fluids*, 2005, **39**, 977.
4 K. Haller, Y. Ventikos, D. Poulikakos and P. Monkewitz, Computational study of high-speed liquid droplet impact, *J. Appl. Phys.*, 2002, **92**, 2821.
5 A. McDonald, M. Lamontagne, C. Moreau and S. Chandra, Impact of plasma-sprayed metal particles on hot and cold glass surfaces, *Thin Solid Films*, 2006, **514**, 212.
6 M. Rein, Phenomena of liquid drop impact on solid and liquid surfaces, *Fluid Dyn. Res.*, 1993, **12**, 61.
7 A. L. Yarin, Drop impact dynamics: splashing, spreading, receding, Bouncing…, *Annu. Rev. Fluid Mech.*, 2006, **38**, 159.
8 D. van Dam and C. Le Clerc, Experimental study of the impact of an ink-jet printed droplet on a solid substrate, *Phys. Fluids*, 2004, **16**, 3403.
9 L. Cheng, Dynamic spreading of drops impacting onto a solid surface, *Ind. Eng. Chem. Process Des. Dev.*, 1977, **16**, 192.
10 C. Clanet, C. Béguin, D. Richard and D. Quéré, Maximal deformation of an impacting drop, *J. Fluid Mech.*, 2004, **517**, 199.
11 R. Bhola and S. Chandra, Parameters controlling solidification of molten wax droplets falling on a solid surface, *J. Mater. Sci.*, 1999, **34**, 4883.
12 R. E. Ford and C. G. L. Furmidge, *Impact and Spreading of Spray Droplets on Foliar Surfaces, Wetting*, Society of Chemical Industry, London, Monograph 25, 1967, p. 417.
13 H. Fukanuma and A. Ohmori, Behavior of Molten Droplets Impinging on Flat Surfaces, *Proc. of the 7th National Thermal Spray Conference*, 1994, vol. 563.
14 H. Marmanis and S. T. Thoroddsen, Scaling of the fingering pattern of an impacting drop, *Phys. Fluids*, 1996, **8**, 1344.
15 C. D. Stow and M. G. Hadfield, An experimental investigation of fluid flow resulting from the impact of a water drop with an unyielding dry surface, *Proc. R. Soc. London, Ser. A*, 1981, **373**, 419.
16 P. Tsai, M. W. Hendrix, R. M. Dijkstra, L. Shui and D. Lohse, Microscopic structure influencing macroscopic splash at high Weber number, *Soft Matter*, 2011, **7**, 11325.
17 T. Tran, H. J. J. Staat, A. Prosperetti, C. Sun and D. Lohse, Drop impact on superheated surfaces, *Phys. Rev. Lett.*, 2012, **108**, 036101.
18 Y. Tagawa, N. Oudalov, C. W. Visser, I. R. Peters, D. van der Meer, C. Sun, A. Prosperetti and D. Lohse, Highly focused supersonic microjets, *Phys. Rev. X*, 2012, **2**(3), 031002.
19 C. T. Chin, C. Lancee, J. Borsboom, F. Mastik, M. E. Frijlink, N. de Jong, M. Versluis and D. Lohse, Brandaris 128: a digital 25 million frames per second camera with 128 highly sensitive frames, *Rev. Sci. Instrum.*, 2003, **74**, 5026.
20 A. van der Bos, A. Zijlstra, E. Gelderblom and M. Versluis, iLIF: illumination by Laser-Induced Fluorescence for single flash imaging on a nanoseconds timescale, *Exp. Fluids*, 2011, **51**, 1283.
21 M. Mani, S. Mandre and M. P. Brenner, Events before droplet splashing on a solid surface, *J. Fluid Mech.*, 2010, **647**, 163.

22 R. C. A. van der Veen, T. Tran, D. Lohse and C. Sun, Direct measurements of air layer profiles under impacting droplets using high-speed colorinterferometry, *Phys. Rev. E: Stat., Nonlinear, Soft Matter Phys.*, 2012, **85**, 026315.
23 W. Bouwhuis, R. C. A. Van der Veen, T. Tran, D. L. Keij, K. G. Winkels, I. R. Peters, D. Van der Meer, C. Sun, J. H. Snoeijer, and D. Lohse, Maximal air bubble entrainment at liquid drop impact, arXiv:1205.4761, 2012.
24 L. Xu, W. Zhang and S. Nagel, Drop splashing on a dry smooth surface, *Phys. Rev. Lett.*, 2005, **94**, 184505.
25 M. M. Driscoll and S. R. Nagel, Ultrafast interference imaging of air in splashing dynamics, *Phys. Rev. Lett.*, 2011, **107**, 154502.
26 S. Mandre and M. P. Brenner, The mechanism of a splash on a dry solid surface, *J. Fluid Mech.*, 2012, **690**, 148.
27 S. Thoroddsen, T. Etoh, K. Takehara, N. Ootsuka and A. Hatsuki, The air bubble entrapped under a drop impacting on a solid surface, *J. Fluid Mech.*, 2005, **545**, 203.
28 J. Eggers, M. Fontelos, C. Josserand and S. Zaleski, Drop dynamics after impact on a solid wall: theory and simulations, *Phys. Fluids*, 2010, **22**, 062101.
29 S. Chandra and C. T. Avedisian, On the collision of a droplet with a solid surface, *Proc. R. Soc. London, Ser. A*, 1991, **432**, 13.
30 S. E. Bechtel, D. B. Bogy and F. E. Talke, Impact of a liquid drop against a flat surface, *IBM J. Res. Dev.*, 1981, **25**, 963.
31 J. Madejski, Solidification of droplets on a cold surface, *Int. J. Heat Mass Transfer*, 1976, **19**, 1009.
32 I. V. Roisman, R. Rioboo and C. Tropea, Normal impact of a liquid drop on a dry surface: model for spreading and receding, *Proc. R. Soc. London, Ser. A*, 2002, **458**, 1411.